# Midlatitude–Equatorial Dynamics of a Grounded Deep Western Boundary Current. Part I: Midlatitude Flow and the Transition to the Equatorial Region

GORDON E. SWATERS

*Institute of Applied Mathematics, Department of Mathematical and Statistical Sciences, and Institute for Geophysical Research, University of Alberta, Edmonton, Alberta, Canada*

(Manuscript received 15 October 2014, in final form 21 May 2015)

ABSTRACT

A comprehensive theoretical study of the nonlinear hemispheric-scale midlatitude and cross-equatorial steady-state dynamics of a grounded deep western boundary current is given. The domain considered is an idealized differentially rotating, meridionally aligned basin with zonally varying parabolic bottom topography so that the model ocean shallows on both the western and eastern sides of the basin. Away from the equator, the flow is governed by nonlinear planetary geostrophic dynamics on sloping topography in which the potential vorticity equation can be explicitly solved. As the flow enters the equatorial region, it speeds up and becomes increasingly nonlinear and passes through two distinguished inertial layers referred to as the ''intermediate'' and ''inner'' inertial equatorial boundary layers, respectively. The flow in the intermediate equatorial region is shown to accelerate and turn eastward, forming a narrow equatorial jet. The qualitative properties of the solution presented are consistent with the known dynamical characteristics of the deep western boundary currents as they flow from the midlatitudes into the tropics. The predominately zonal flow across the ocean basin in the inner equatorial region (and its exit from the equatorial region) is determined in Part II of this study.

## 1. Introduction

The deep western boundary currents (DWBCs) in the Atlantic Ocean are an important pathway for the equatorward flow of deep cold waters produced in the Labrador and Norwegian/Greenland Seas. In midlatitudes, these currents correspond to grounded equatorward flows on a sloping bottom with distinct upslope and downslope incroppings or groundings (locations where the isopycnal or height field intersects the bottom; e.g., see Fig. 3 in Toole et al. 2011). (It is important to point out that while our work here explicitly assumes a DWBC that has both an upslope and downslope grounding, not all sections of the DWBC possess this property.) Although some of the water associated with the DWBC mixes with the overlying ocean in the Northern Hemisphere and returns poleward, the core of the DWBC continues to flow southward where it eventually encounters and crosses the equator (e.g., Baehr et al. 2009; Cunningham et al. 2007; Fischer and Schott 1997; McCartney 1993; McCartney and Curry 1993). A similar dynamical picture holds for the deep water produced in Antarctica that flows northward along the east coast of South America (e.g., McCartney and Curry 1993; Choboter and Swaters 2004).

Oceanographic observations (e.g., Fischer and Schott 1997; Thierry et al. 1998; Richardson and Fratantoni 1999; Gouriou et al. 2001; Dengler et al. 2004) of the DWBC in the equatorial region suggest the following dynamical scenario. As the equator is approached, current speeds in the DWBC increase and are maximum at the equator. The DWBC enters the equatorial region at about 44°W southeast of French Guiana. While some of the water associated with the DWBC continues to flow southward along the coast of Brazil where it breaks up into eddies at about 8°S, the bulk of the DWBC water mass separates from the South American coast at about 3°S, 35°W and turns eastward, flowing ''swiftly'' along the equator. The flow along the equator occurs in a fairly narrow ±3° latitudinal band in a topographically constrained equatorial channel located northward of a line of seamounts located along the Fernando de Noronha Ridge. The deepest or abyssal currents in the equatorial

*Corresponding author address:* Gordon E. Swaters, Department of Mathematical and Statistical Sciences, University of Alberta, 632 Central Academic Building, Edmonton AB T6G2G1, Canada. E-mail: gswaters@ualberta.ca

DOI: 10.1175/JPO-D-14-0207.1

channel exhibit meridional oscillations with a wavelength ''roughly'' on the order of 1000 km. While the Mid-Atlantic Ridge somewhat disrupts the eastward flow, some of the DWBC water makes its way into the Gulf of Guinea, where it is deflected to the south and flows along Africa, ultimately making its way into the Indian Ocean and eventually the Pacific Ocean, where it upwells and becomes part of the surface circulation.

The principal purpose of this paper is to present a coherent comprehensive analytical theory that is able to reproduce the qualitative dynamical features described above for the midlatitude–cross-equatorial flow of a grounded DWBC in a highly idealized ocean basin and topography model. It is worth pointing out that the present generation of OGCMs is incapable of resolving the dynamical detail the above observations suggest. Specifically, we give a leading-order kinematic description of the steady nonlinear cross-equatorial flow of a DWBC in a meridional channel that spans the equator with parabolic bottom topography (so that the model ocean shallows on both the eastern and western sides). Included in our description is the complete determination of the flow as a function of latitude in midlatitudes and the nonlinear structure of the pathlines in the equatorial region. Our presentation of the theory is broken up into two parts. This paper, called Part I, presents the intrinsically nonlinear dynamics of the DWBC as it flows equatorward in midlatitudes along the western sloping boundary across the planetary vorticity gradient and the dynamics of the DWBC as it begins to enter the equatorial region and turns eastward. Swaters (2015, hereinafter Part II) examines the highly nonlinear predominately zonal flow along the equator and its ultimate exit from the equatorial region on the eastern boundary.

Shallow water modeling of DWBCs suggests that away from the equator the dominant contribution to the potential vorticity (PV) is planetary vorticity and the baroclinic stretching associated with the current thickness with the relative vorticity making a secondary contribution (Edwards and Pedlosky 1998a,b; Choboter and Swaters 2004), implying that in midlatitudes the leading-order dynamical balance is described by a planetary geostrophic approximation. As pointed out by Edwards and Pedlosky (1998a,b), in order that a current be in planetary geostrophic balance on either side of the equator, the cross-equatorial flow must involve nonconservative processes such as dissipation since the Coriolis parameter changes sign at the equator.

Nof and Borisov (1998) examined the cross-equatorial flow of a grounded current in a meridional channel with parabolic bottom topography. Their analytical modeling was based on assuming that the flow away from the equator possessed constant PV with a DWBC height field and geostrophically balanced velocity with an ad hoc parametric dependence on latitude. Our goal in Part I is to construct a fully self-consistent theory for the midlatitude flow of a DWBC on sloping topography that crosses the planetary vorticity gradient and as it enters the equatorial region. Nof and Borisov (1998) did not determine the structure of the flow in the equatorial region. Numerical simulations presented by Nof and Borisov (1998) suggested that while the flow in the equatorial region was largely inertial, as the flow progressed internal frictional sublayers develop, and this allows the required PV modification to occur for cross-equatorial flow.

The outline of this paper is as follows. In section 2, the reduced-gravity model is introduced and nondimensionalized with midlatitude scalings. In section 3 the leading-order flow in midlatitudes is explicitly determined. The flow is in planetary geostrophic balance and the leading-order PV equation is shown to reduce to a quasi-linear hyperbolic equation for the DWBC height that can be explicitly solved using the method of characteristics. Among other properties it is shown that the midlatitude solution for the DWBC height decreases and the zonal and equatorward speeds progressively increase as the equator is approached, all within the context of conserving meridional volume transport. The midlatitude results suggest the emergence of an ''intermediate'' nonlinear inertial equatorial boundary layer with width on the order of about 885 km centered on the equator.

Section 4 describes the solution for the DWBC in the intermediate equatorial region. Within this intermediate region, the leading-order problem for the DWBC can be solved exactly. It is in this intermediate region that the DWBC turns eastward along the equator. The DWBC within this intermediate region continues to speed up and the height continues to decrease, resulting in a ''narrow'' zonally aligned equatorial jet being formed. This suggests the emergence of an ''inner'' nonlinear inertial equatorial boundary layer with width on the order of about 221 km centered on the equator in order to resolve the flow of the DWBC along the equator. The paper is summarized in section 5 and the stage is set for the work in Part II.

## 2. Governing equations

Although it is possible to work in spherical coordinates (as in Swaters 2013), it is more convenient to work with the nonlinear steady reduced-gravity shallow-water equations with variable bottom topography for a differentially rotating fluid in Cartesian coordinates written in the form (Pedlosky 1987)

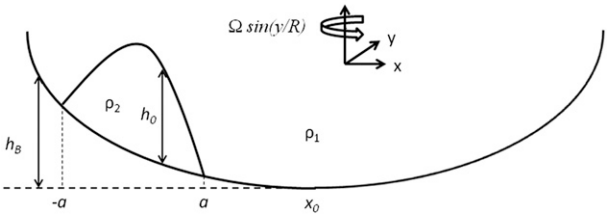


FIG. 1. Geometry of the abyssal height $h_0(x)$ along $y = y_0$.

$$(u\partial_x + v\partial_y)u - 2\Omega\sin(y/R)v = -g'(h + h_B)_x + A_H\Delta u, \tag{1}$$

$$(u\partial_x + v\partial_y)v + 2\Omega\sin(y/R)u = -g'(h + h_B)_y + A_H\Delta v, \tag{2}$$

and

$$(uh)_x + (vh)_y = 0, \tag{3}$$

where $x$ and $y$ are the eastward and northward coordinates, respectively, with corresponding velocities $u(x, y)$ and $v(x, y)$, respectively; $h(x, y) > 0$ is the height of the DWBC above the topography $h_B(x)$ (which we assume only varies in the zonal direction $x$); $g' = g(\rho_2 - \rho_1)/\rho_2 > 0$ is the stably stratified reduced gravity where $\rho_1$ is the density of the assumed infinitely deep and quiescent overlying water column and $\rho_2$ is the density of the DWBC (see Fig. 1); $\Omega = 2\pi$ rad day$^{-1}$ is the angular frequency of Earth's rotation; $R \simeq 6400$ km is the radius of the Earth; and $A_H$ is a horizontal eddy viscosity coefficient. The usual equatorial $\beta$-plane approximation is not made on account of the fact that we want to have a realistic (bounded) magnitude of the Coriolis parameter in midlatitudes "far away" from the equator (see, e.g., Choboter and Swaters 2004). The reduced pressure in the DWBC associated with this model is simply $p = \rho_2 g'(h + h_B)$.

Equations (1)–(3) will be solved assuming that at $y = y_0 > 0$ (located in northern midlatitudes away from the equator) the flow is geostrophically balanced and that

$$h(x, y_0) = h_0(x) \equiv \begin{cases} H_*(1 - x^2/a^2) & \text{when} \quad |x| \le a, \\ 0 & \text{when} \quad |x| > a, \end{cases} \tag{4}$$

where $H_*$ is the maximum height or thickness of the DWBC located at the point $x = 0$ and $a > 0$ is the DWBC half-width located along $y = y_0$. The height [(4)] contains two groundings or incroppings located at $x = \pm a$, respectively.

The bottom topography is the parabolic profile given by

$$h_B = \gamma(x_0 - x)^2, \tag{5}$$

where $x_0 > a$ is the zonal location of the point of maximum depth located to the east of the downslope grounding associated with $h_0(x)$ (see Fig. 1), and $\gamma > 0$ is a parameter that is chosen so that the average value of the topographic slope immediately under $h_0(x)$ is reasonably consistent with observations of the underlying bottom slope associated with the DWBC (Swaters 2006a,b) in midlatitudes, that is,

$$\frac{1}{2a}\int_{-a}^{a} h_B'(x)\,dx = -s < 0 \Rightarrow \gamma = s/(2x_0), \tag{6}$$

where $s > 0$ is the slope parameter. In the real ocean, of course, the eastern and western boundaries of the domain as well as bottom topography are a function of latitude. We have taken the highly idealized approximation of assuming that the bottom topography varies only in the zonal direction in order to focus attention on the theoretical dynamics of the equatorward flow of a grounded abyssal current along a sloping bottom without the additional complexity of highly irregular meridionally dependent bottom bathymetry.

Figure 1 illustrates the geometry and the flow and topographic configuration along $y = y_0$. To clearly see all aspects of the configuration, not all items in Fig. 1 are in relative scale to each other. For example, the height of the DWBC is greatly exaggerated in comparison to the half-width because, in reality, $H_* \ll a$. In addition, the point of maximum depth is significantly displaced from the downslope grounding, that is, $x_0 \gg a$. Figure 1 shows the qualitative situation. It is not meant to be taken literally.

Our analysis is facilitated by the introduction of the following nondimensional (tilde) variables given by

$$\left.\begin{aligned} x = L\tilde{x}, \quad (y, y_0) = R(\tilde{y}, \tilde{y}_0), \quad v = V\tilde{v}, \quad u = (VL/R)\tilde{u}, \\ (h, h_B, h_0) = (2\Omega VL/g')(\tilde{h}, \tilde{h}_B, \tilde{h}_0), \quad p = 2\Omega VL\rho_2\tilde{p}, \end{aligned}\right\}, \tag{7}$$

where $L = a$ is the zonal length scale and $V = V_{\text{nof}} \equiv sg'/(2\Omega)$ is the meridional velocity scale where $V_{\text{nof}}$ is the Nof speed (Nof 1983), which is the speed of a steady gravity-driven geostrophically balanced grounded abyssal water mass on a sloping bottom, which will be the dominant dynamical balance outside the equatorial region. The zonal velocity is scaled so that both the zonal and meridional volume fluxes balance each other in the mass conservation equation [(3)]. The meridional length scale is taken to the Earth's radius $R$ in recognition that the flow outside the equatorial region is hemispheric in scale. Finally, the DWBC height $h$, the topography $h_B$, the boundary condition $h_0$, and the reduced pressure $p$ are all geostrophically scaled.

Substitution of (7) into (1)–(5) yields the nondimensional equations, after dropping the tildes, given by

$$\varepsilon\kappa^2(u\partial_x + v\partial_y)u - \sin(y)v = -(h+h_B)_x + \frac{\varepsilon}{R_E}(\partial_{xx} + \kappa^2\partial_{yy})u, \quad (8)$$

$$\varepsilon(u\partial_x + v\partial_y)v + \sin(y)u = -h_y + \frac{\varepsilon}{\kappa^2 R_E}(\partial_{xx} + \kappa^2\partial_{yy})v, \quad (9)$$

and

$$(uh)_x + (vh)_y = 0, \quad (10)$$

where the reduced pressure is $p = h + h_B$, and where

$$h(x, y_0) = h_0(x) \equiv \begin{cases} H(1-x^2) & \text{when} \quad |x| \le 1, \\ 0 & \text{when} \quad |x| > 1, \end{cases} \quad \text{and} \quad (11)$$

$$h_B(x) = \frac{1}{2\delta}(1-\delta x)^2 \Rightarrow h_B'(x) = -1 + \delta x, \quad (12)$$

with

$$\varepsilon \equiv \frac{g's}{4a\Omega^2}, \quad \kappa \equiv \frac{a}{R}, \quad H \equiv \frac{H_*}{sa}, \quad \delta \equiv \frac{a}{x_0}, \quad \mathrm{Re} \equiv \frac{RV}{A_H}, \quad (13)$$

where $\varepsilon$ is the Rossby number, $\kappa$ is the aspect ratio between the zonal and meridional length scales, $H$ is the nondimensional maximum height of the boundary condition $h_0(x)$, $\delta^{-1}$ is the nondimensional position of the point of maximum depth, and Re is the Reynolds number.

Typical values for the parameters appropriate for the DWBC are

$$g' \simeq 10^{-3}\,\mathrm{m\,s^{-2}}, \quad s \simeq 5.6\times10^{-3}, \quad a \simeq 100\,\mathrm{km}, \quad A_H \simeq 10^2\,\mathrm{m^2\,s^{-1}}, \quad (14)$$

which implies that the meridional and zonal velocity scalings are, respectively,

$$V_{\mathrm{nof}} \simeq 3.9\,\mathrm{cm\,s^{-1}} \quad \text{and} \quad V_{\mathrm{nof}}L/R \simeq 0.06\,\mathrm{cm\,s^{-1}}, \quad (15)$$

suggesting that

$$\varepsilon \simeq 2.6\times10^{-3}, \quad \kappa \simeq 1.6\times10^{-2}, \quad \mathrm{Re} \simeq 2464, \quad (16)$$

which suggests that

$$O(\varepsilon^2) \lesssim \kappa^2 \simeq \mathrm{Re}^{-1} \lesssim O(\varepsilon).$$

In addition, the DWBC height scale would be approximately

$$sa \simeq 560\,\mathrm{m} \Rightarrow H \simeq O(1), \quad (17)$$

and assuming that (at least) $x_0 \simeq 1000\,\mathrm{km}$, it follows that

$$O(\varepsilon) < \delta = 10^{-1} < 1. \quad (18)$$

In what follows, we assume the Rossby number $\varepsilon$ as the underlying asymptotic parameter. Equations (8)–(12) may be thought of as the midlatitude or "outer" asymptotic problem in the limit $0 < \varepsilon \ll 1$.

## 3. The flow in midlatitudes

The leading-order (as $\varepsilon \to 0$) dynamics of the DWBC in midlatitudes where $y \simeq O(1)$ will be given by the nonlinear planetary geostrophic balance:

$$v = \frac{1}{\sin y}(h + h_B)_x, \quad (19)$$

$$u = -\frac{1}{\sin y}h_y, \quad (20)$$

$$(uh)_x + (vh)_y = 0, \quad \text{and} \quad (21)$$

$$p = h + h_B, \quad (22)$$

with the boundary condition

$$h(x, y_0) = h_0(x). \quad (23)$$

Substitution of (19) and (20) into (21) yields the quasi-linear hyperbolic equation

$$\tan(y)h_y - \frac{h}{h_B'(x)}h_x = h. \quad (24)$$

Equation (24) is the Cartesian analog of the spherical coordinate equation [(5a)] in Swaters (2013). Equation (24) is simply the PV equation associated with (19)–(21) given by

$$(u, v)\cdot\nabla\left(\frac{\sin y}{h}\right) = 0. \quad (25)$$

The solution to (24) subject to (23), obtained via the method of characteristics (for details see Swaters 2013), is given by

$$h(x, y) = \frac{\sin y}{\sin y_0}h_0(\tau), \quad \text{and} \quad (26)$$

$$h_B(\tau) + \left(\frac{\sin y_0 - \sin y}{\sin y_0}\right)h_0(\tau) = h_B(x). \quad (27)$$

Given the coordinates $(x, y)$, the characteristic coordinate $\tau(x, y)$ is obtained from (27) [assuming that $\tau(x, y_0) = x$] and $h(x, y)$ is then obtained from (26). It is

worth commenting that the solution [(26) and (27)] is one of the very few exact analytical solutions known for inertial meridional flow that crosses the planetary vorticity gradient. We also note that the solution [(26) and (27)] does not, as must be the case, correspond to a parallel shear flow.

The individual velocity components $u$ and $v$ can be written in the form

$$u(x,y) = -\frac{p_y}{\sin y} = -\frac{\tau_y}{\sin y}[h_0'(\tau) + h_B'(\tau)] = \frac{\cot(y)h_0(\tau)[h_0'(\tau) + h_B'(\tau)]}{\sin(y_0)h_B'(\tau) + (\sin y_0 - \sin y)h_0'(\tau)}, \quad \text{and} \quad (28)$$

$$v(x,y) = \frac{p_x}{\sin y} = \frac{\tau_x}{\sin y}[h_0'(\tau) + h_B'(\tau)] = \frac{\sin(y_0)h_B'(x)[h_0'(\tau) + h_B'(\tau)]}{\sin(y)[\sin(y_0)h_B'(\tau) + (\sin y_0 - \sin y)h_0'(\tau)]}, \quad (29)$$

where (27) has been used and "prime" means differentiation with respect to the argument.

For $h_0(x)$ and $h_B(x)$ given by (11) and (12), respectively, $\tau(x,y)$ can be explicitly determined from (27) and is given by

$$\tau(x,y) = \begin{cases} \Upsilon(x,y) & \text{for} \quad |x| \le 1, \\ x & \text{for} \quad |x| > 1, \end{cases} \quad (30)$$

where

$$\Upsilon(x,y) \equiv \frac{1 - \sqrt{1 + 2\left[\frac{2(\sin y_0 - \sin y)H}{\sin y_0} - \delta\right]\left[x - \frac{\delta x^2}{2} + \frac{(\sin y_0 - \sin y)H}{\sin y_0}\right]}}{\delta - 2(\sin y_0 - \sin y)H/\sin y_0}. \quad (31)$$

We remark that while we are working from the framework of an equatorward flowing grounded current in the Northern Hemisphere, the solutions (26)–(29) are equally valid for an equatorward flowing grounded current in the Southern Hemisphere on the western side of a basin. All that is required is to map $(y, y_0) \to (-y, -y_0)$. In such a case we see that $h(x, y)$, $u(x, y)$, and $\tau(x, y)$ are unchanged, that is, are invariant, but that $v \to -v$ (the current flows, of course, northward instead of southward).

### a. *General properties of the midlatitude solution*

There are several important properties associated with the midlatitude solution [(26) and (27)] irrespective of the specific $h_0(x)$ and $h_B(x)$ assumed. The first property to note is that the characteristics [the curves for which $\tau(x, y)$ is constant] are coparallel with the geostrophic streamlines [the curves for which $p(x, y)$ is constant] since it follows from (22) and (27) that

$$p(x,y) = h(x,y) + h_B(x) = h_0(\tau) + h_B(\tau). \quad (32)$$

The second property is that the streamlines are oriented in the southwest-to-northeast direction. We have

$$\left.\frac{dy}{dx}\right|_{\tau=\text{constant}} = -\frac{\tau_x}{\tau_y} = -\frac{\sin(y_0)h_B'(\tau)}{\cos(y)h_0(\tau)} > 0, \quad (33)$$

since we assume an equatorward flow in the Northern Hemisphere on the western side of a basin, that is, $\sin(y_0) > 0$ and $h_B'(\tau) < 0$ [clearly, $\cos(y)$ and $h_0(\tau)$ are both positive in the interior of the flow]. Consequently, the solution [(26) and (27)] will have the property that there will be a (slight) upslope component of the flow as it moves equatorward. This as a consequence of the planetary vorticity gradient that creates a tendency for westward or upslope deflection in the flow as it moves southward.

The third property is that the cross-slope position of the groundings will be *independent* of latitude $y$. To see this, consider the possibility that a grounding *does* depend on latitude and is given by $x = \tilde{x}(y)$ with $\tilde{x}(y_0) = \alpha$, where $h_0(\alpha) = 0$ is set by the boundary condition, that is, $h[\tilde{x}(y), y] = 0$ for all $y$. It then follows from (26) that

$$h[\tilde{x}(y), y] = \frac{\sin y}{\sin y_0} h_0[\tau(\tilde{x}, y)] = 0 \Rightarrow h_0[\tau(\tilde{x}, y)] = 0, \quad (34)$$

which, when inserted into (27), implies

$$h_B[\tau(\tilde{x}, y)] = h_B(\tilde{x}) \Rightarrow \tau(\tilde{x}, y) = \tilde{x} \Rightarrow h_0(\tilde{x}) = 0 \Rightarrow \tilde{x} = \alpha, \quad (35)$$

which is independent of $y$. Thus, in the midlatitude region of the flow, the cross-slope position of the groundings in the interior will be set by their location along the northern boundary and their cross-slope position does not vary as the DWBC flows equatorward.

The fourth property is that it follows from (26), (28), and (29) that, respectively,

$$\lim_{y \to 0^+} h(x,y) = 0, \quad \text{and} \quad (36)$$

$$\lim_{y \to 0^+} |u| = \lim_{y \to 0^+} |v| = \infty. \quad (37)$$

The limit in (36) can be understood as a consequence of the invariance of the planetary geostrophic PV along the

streamlines as seen in (25). The "singularity" in $u$ and $v$ is properly understood as a consequence of the mass conservation equation [(21)] that suggests that the volume fluxes are bounded even though $h(x, y) \to 0$ as $y \to 0$. The midlatitude solution [(26) and (27)] possesses the property that, consistent with the observations, the DWBC speeds up as the equator is approached.

It follows from the continuity equation [(21)] that the meridional transport is constant with respect to $y$. We can explicitly calculate the meridional transport in terms of the boundary condition and bottom topography as follows. Suppose that the DWBC height is nonzero over the interval $x_1 \le x_2$ with $h(x_{1,2}, y) = 0$. If we denote the meridional transport as $T_y$, it follows that

$$\begin{aligned} T_y &\equiv \int\int_{x1}^{x2} h(x,y)v(x,y)\,dx = \int_{x_1}^{x_2} \frac{h(x,y)p_x(x,y)}{\sin y}\,dx \\ &= \frac{1}{\sin y_0}\int_{x_1}^{x_2} h_0(\tau)[h_0'(\tau)+h_B'(\tau)]\tau_x\,dx \\ &= \frac{1}{\sin y_0}\int_{\tau(x_1,y)}^{\tau(x_2,y)} h_0(\tau)[h_0'(\tau)+h_B'(\tau)]\,d\tau \\ &= \frac{1}{\sin y_0}\int_{x_1}^{x_2} h_0(\tau)[h_0'(\tau)+h_B'(\tau)]\,d\tau = \frac{1}{\sin y_0}\int_{x_1}^{x_2} h_0(\tau)h_B'(\tau)\,d\tau, \end{aligned} \tag{38}$$

where (27), (29), (34), and (35) have been used. Note that it follows from (26), (28), and (29) that the meridional and zonal volume fluxes given by $h(x, y)v(x, y)$ and $h(x, y)u(x, y)$, respectively, will be bounded continuous functions with respect to $y$ over the entire interval $0 \le y \le y_0$.

The final property we want to establish is that if the meridional velocity associated with the northern boundary condition is everywhere equatorward, that is, $v(x, y) < 0$, then no shock will form in the solution before it encounters the equator. That is, it is physically meaningful to think of (26) and (27) as extending to the outer limits of the equatorial region. This last property is very important to establish since if it does not hold, the entire theory would be of very limited value because (26) and (27) would not extend into the equatorial region.

A shock will occur in the solution [(26) and (27)] when the characteristics curves intersect and this will occur when $|h_x| \to \infty$. It follows that

$$h_x = \frac{\sin y}{\sin y_0}h_0'(\tau)\tau_x = \frac{\sin(y)h_B'(\tau)h_0'(\tau)}{\sin(y_0)h_B'(\tau)+(\sin y_0-\sin y)h_0'(\tau)}, \tag{39}$$

where (27) has been used. We see that if the denominator in (39) is zero, then $|h_x| \to \infty$. Consequently, if the coordinates of the shock line are denoted as $(x_s, y_s)$, then it follows from (39) and (27) that

$$\begin{aligned} \frac{\sin y_s}{\sin y_0} &= \frac{h_B'(\tau)+h_0'(\tau)}{h_0'(\tau)}, \\ h_B(x_s) &= h_B(\tau) - \frac{h_0(\tau)h_B'(\tau)}{h_0'(\tau)}. \end{aligned} \tag{40}$$

We note that if a shock forms in the solution, it follows from (28) and (29) that $|u(x_s, y_s)| \sim |v(x_s, y_s)| \to \infty$, which we argue is physically unacceptable.

Since we are implicitly assuming that the current is "initially" located where $h_B'(\tau) < 0$ (on the western side of the basin), it necessarily follows from (40) that the shock, if it exists in the region $0 < y < y_0$, must occur where $h_0'(\tau) > 0$ since

$$h_0'(\tau) < 0 \Rightarrow [h_B'(\tau)+h_0'(\tau)]/h_0'(\tau) > 1 \Rightarrow y_s > y_0,$$

which is not physically interesting (i.e., the shock forms north of our boundary condition and is not in the region of interest). If a shock forms in the region $0 < y < y_0$, it must therefore develop on the upslope side of the equatorward flowing DWBC and not on the downslope side. The only possibility that a shock can develop in the region $0 < y < y_0$ is if there exists $\tau$ values for which

$$\begin{aligned} &0 < [h_B'(\tau)+h_0'(\tau)]/h_0'(\tau) < 1 \quad \text{and} \quad h_0'(\tau) > 0 \\ &\quad \Rightarrow h_B'(\tau)+h_0'(\tau) > 0. \end{aligned}$$

Consequently, should it be the case that

$$h_B'(\tau)+h_0'(\tau) < 0 \quad \text{for all} \quad \tau, \tag{41}$$

within the DWBC, then *no shock can form* in the region $0 < y < y_0$, which is the domain of interest.

Condition (41) has a very simple physical interpretation. From (39) the meridional velocity along $y = y_0$ is given by

$$v(x, y_0) = \frac{h_0'(x)+h_B'(x)}{\sin(y_0)}. \tag{42}$$

Thus, if the meridional velocity within the DWBC is everywhere equatorward along the boundary $y = y_0$, no shock will form in the solution in the region $0 < y < y_0$ and the DWBC solution [(26) and (27)] will extend to but not fully into the equatorial region. Conversely, if the meridional velocity along the northern boundary contains a poleward component, the midlatitude solution presented here necessarily contains a shock and the solution [(26) and (27)] breaks down before it enters the equatorial region. (Of course, should a shock form, it is always possible to formally construct a "weak" solution using the appropriate Rankine–Hugoniot conditions. However, we would argue that while mathematically correct, such a discontinuous solution is not physically relevant because dissipative processes would induce mixing along the shock line that would reestablish a predominantly equatorward flow in any event.)

There is very good pointwise agreement between the analytical solution described above and the time-averaged height and a velocity field associated with the fully nonlinear shallow water initial-value numerical simulations described by Kim et al. (2014) for equator-crossing grounded abyssal flow in midlatitudes away from the equator. Moreover, the three specific properties associated with our midlatitude solution suggesting that the DWBC speeds up, the thickness diminishes, and that there is an essential upslope flow component as the DWBC crosses the planetary vorticity gradient is consistent with the Miami Isopycnic Coordinate Model (MICOM) simulations presented by Spall (1994).

### b. *Description of the midlatitude solution with specific parameters*

To provide a graphical description of the midlatitude solution, specific parameter values for the solution [(26) and (27)] are needed. We assume that

$$y_0 = \pi/4, \tag{43}$$

$$H_* = 300\,\text{m} \Rightarrow H \simeq 0.54, \quad \text{and} \tag{44}$$

$$a = 100\,\text{km} \quad \text{and} \quad x_0 = 1000\,\text{km} \Rightarrow \delta = 0.1. \tag{45}$$

These parameter values will ensure that the meridional velocity along the northern boundary is everywhere equatorward, that is,

$$v(x, y_0) = \frac{(\delta - 2H)x - 1}{\sin(\pi/4)} < 0 \quad \text{for all} \quad -1 \le x \le 1. \tag{46}$$

Figure 2a is a graph of the DWBC height $h_0(x)$ on the topography $h_B(x)$ along $y = y_0$ versus $x$ for $-2 \le x \le 22$ for the parameter values given above. Unlike Fig. 1, within this figure the DWBC current height and bottom topography are shown in proportionate scale to each other. Fig. 2b is a "close up" graph of the meridional velocity $v(x, y_0)$ along $y = y_0$ versus $x$ for $-1.5 \le x \le 1.5$ for the parameter values given above.

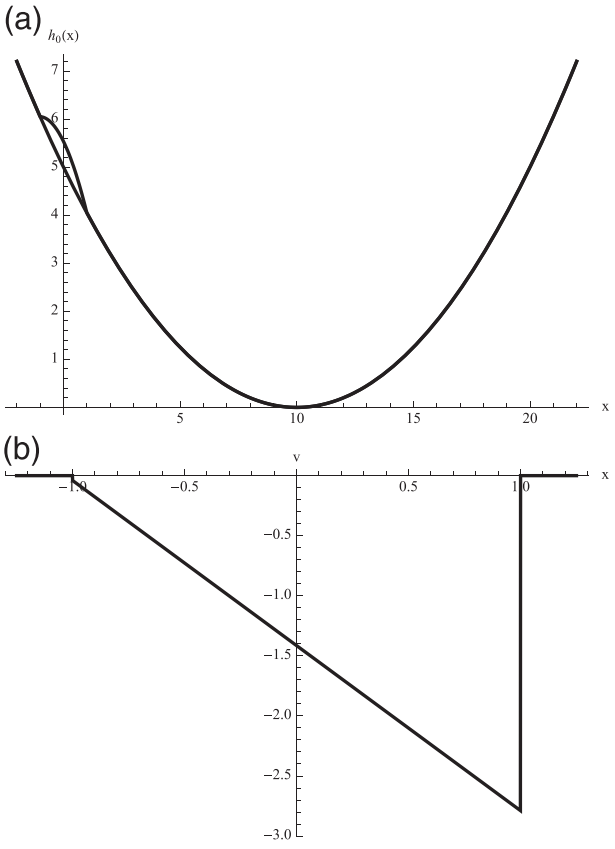


FIG. 2. Along $y = y_0$, (a) $h_0(x)$ on the topography $h_B(x)$ and (b) meridional velocity $v(x, y_0)$.

Figure 3 is a contour plot of the characteristics $\tau(x, y)$ as determined by (30) and (31) for $\tau = -1$ to $+1$ in 0.25 increments over the region $-1 < x < 1$ and $0 < y < \pi/4$. The solid lines will also correspond to the geostrophic streamlines for the steady flow. The gray-shaded region is where $h(x, y) > 0$. The flow is predominately equatorward but there is a small upslope component. It is important to remember that the scalings for $x$ and $y$ are quite different so that whereas the span in $y$ shown in Fig. 3 is approximately 5027 km, the distance from $x = -1$ to $x = 1$ corresponds to 200 km. The contours along $x = -1$ and $x = 1$, for which $\tau = -1$ and $\tau = 1$, correspond to the upslope and downslope groundings, respectively. The location of the groundings does not vary with $y$ in accordance with (34) and (35).

Figure 4a is a contour plot of $h(x, y)$ over the region $-1 < x < 1$ and $0 < y < \pi/4$ with a contour interval of about 0.1. The height increases with the

darker shading. The DWBC height decreases approximately linearly as one moves equatorward, although there is clearly some westward intensification. Physically, this west-to-east asymmetry is a consequence of DWBC water ''piling'' up on the upslope flank of the current as the flows moves equatorward and westward.

The approximately linear decrease in the DWBC height as the flow moves equatorward can be seen in Fig. 4b, which is a graph of the zonally averaged DWBC height denoted by $\overline{h}(y)$, given by

$$\overline{h}(y) = \frac{1}{2}\int_{-1}^{1} h(x,y)\,dx, \tag{47}$$

versus $y$ for $0 \le y \le y_0$, where $h(x, y)$ is given by (26) and (27).

From Fig. 3 one can discern that qualitatively $u \le 0$ and $v \le 0$ everywhere within the DWBC. Figures 5a and 5b show the graphs of the zonally averaged zonal and meridional velocities, denoted by $\overline{u}(y)$ and $\overline{v}(y)$, respectively, and given by

$$\overline{u}(y) = \frac{1}{2}\int_{-1}^{1} u(x,y)\,dx, \quad \text{and} \tag{48}$$

$$\overline{v}(y) = \frac{1}{2}\int_{-1}^{1} v(x,y)\,dx, \tag{49}$$

where $u(x, y)$ and $v(x, y)$ are given by (28) and (29), respectively, versus $y$ for $0.02 \le y \le y_0$. The graphs do not extend to $y = 0$ since $u(x, y)$ and $v(x, y)$ both become unbounded as the equator is approached.

As can be seen in Fig. 5, both $\overline{u}(y)$ and $\overline{v}(y)$ vary slowly until about $y \simeq 0.2$, whereupon the velocities rapidly diverge. That is, the rapid increase occurs ''near'' the equator consistent with the observations.

Again, it is important to remember that there are very different scalings associated with $\overline{u}(y)$ and $\overline{v}(y)$ with $\overline{v} = 1$ corresponding to about $4\,\mathrm{cm\,s^{-1}}$ and $\overline{u} = 1$ corresponding to about $0.06\,\mathrm{cm\,s^{-1}}$.

The meridional transport is constant with respect to $y$ and is given by [see (38)]

$$T_y = \frac{1}{\sin(\pi/4)}\int_{-1}^{1} h_0(x)h_B'(x)\,d\tau = -\frac{4H}{3\sin(\pi/4)} \simeq -1.01, \tag{50}$$

which, dimensionally, corresponds to about 2.2 Sv ($1\,\mathrm{Sv} \equiv 10^6\,\mathrm{m^3\,s^{-1}}$) equatorward. This is reasonably consistent with observations of the ''deep'' transport associated with ''overflow/lower deep water'' associated with the DWBC near Cape Cod (e.g., Joyce et al. 2005).

The zonal transport is not, however, constant and is a function of $x$. If we denote the zonal transport by $T_x$, it follows that

$$\begin{aligned} T_x(x) &= \int_0^{y_0} h(x,y)u(x,y)\,dy = -\int_0^{y_0} \frac{h(x,y)p_y(x,y)}{\sin y}\,dy \\ &= -\frac{1}{\sin y_0}\int_0^{y_0} h_0(\tau)[h_0'(\tau) + h_B'(\tau)]\tau_y\,dy \\ &= -\frac{1}{\sin y_0}\int_{\tau(x,0)}^{\tau(x,y_0)} h_0(\tau)[h_0'(\tau) + h_B'(\tau)]\,d\tau \\ &= \frac{1}{\sin y_0}\left\{\frac{h_0^2[\tau(x,0)] - h_0^2(x)}{2} - \int_{\tau(x,0)}^{x} h_0(\tau)h_B'(\tau)\,d\tau\right\}, \end{aligned} \tag{51}$$

where (26) and (28) have been used as well as the fact that $\tau(x, y_0) = x$.

If (11) and (12) are substituted into (51), it follows that

$$T_x(x) = \frac{H}{\sin y_0}\left\{x - \tilde{\tau}(x) + \frac{\tilde{\tau}^3(x) - x^3}{3} + \frac{\delta - 2H}{2}\left[\frac{x^4 - \tilde{\tau}^4(x)}{2} + \tilde{\tau}^2(x) - x^2\right]\right\}, \tag{52}$$

where

$$\tilde{\tau}(x) \equiv \tau(x,0) = \begin{cases} \dfrac{1 - \sqrt{1 + 2(2H - \delta)(H + x - \delta x^2/2)}}{\delta - 2H} & \text{for} \quad |x| \le 1, \\ x & \text{for} \quad |x| > 1, \end{cases} . \tag{53}$$

It follows from (52) that $T_x(\pm 1) = 0$ as it must along the groundings since the groundings are also streamlines [note that $\tilde{\tau}(\pm 1) = \pm 1$] and consequently $u(\pm 1, y) = 0$.

Figure 6 is a graph of the zonal transport within the DWBC over the interval $-1 \le x \le 1$. We see that the zonal transport is everywhere westward within the DWBC and is zero at the groundings. Dimensionally, $T_x = 1$ corresponds to about 2.2 Sv (but remember that this is spread over about 5027 km in latitude) so that the maximum zonal transport, located slightly to the west of the meridional line $x = 0$, is about 0.9 Sv in the upslope direction. To the best of our knowledge, there is no

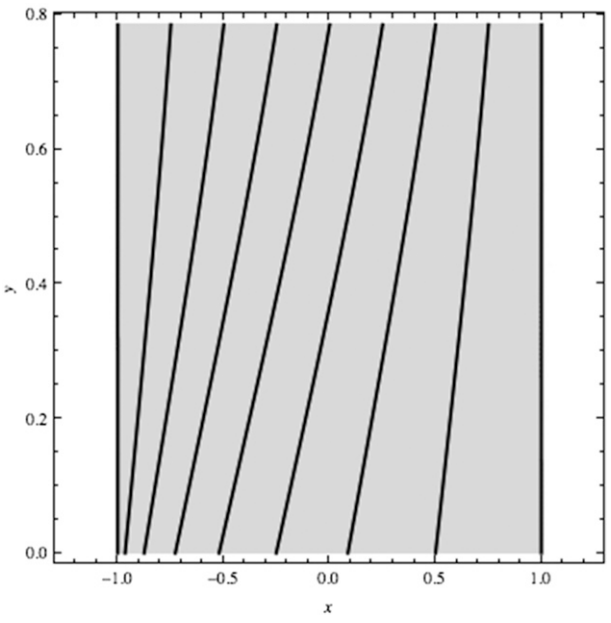


FIG. 3. Contour plot of $\tau(x, y)$ for $\tau = -1$ to $+1$ in 0.25 increments.

observational evidence in support of or disproving this feature of our solution. Namely, that as DWBCs flow toward the equator, all else being equal, our solution suggests that there is tendency toward upslope motion as a consequence of the planetary vorticity gradient.

## 4. The intermediate equatorial region

The midlatitude or "outer" solutions [(26)–(29)] have the leading-order behavior

$$h(x,y) \approx \frac{y h_0[\tilde{\tau}(x)]}{\sin y_0}, \tag{54}$$

$$u(x,y) \approx -\frac{h_0[\tilde{\tau}(x)]}{y \sin y_0}, \quad \text{and} \tag{55}$$

$$v(x,y) \approx \frac{h_B'(x)}{y}, \tag{56}$$

as $y \to 0$, where $\tilde{\tau}(x)$ is given by (53). Although there is no explicit reference to the DWBC height in (56), it is implicitly understood that (56) will only make physical sense within the context that $h(x, y) > 0$. We see that the velocities become progressively unbounded as $y \to 0$. Perhaps surprisingly, (55) suggests that the midlatitude zonal velocity becomes increasingly westward as the equatorial region is initially encountered. The midlatitude solution for the DWBC height [(54)] exhibits a linear decrease with respect to $y$ as $y \to 0$. Nevertheless, the leading-order

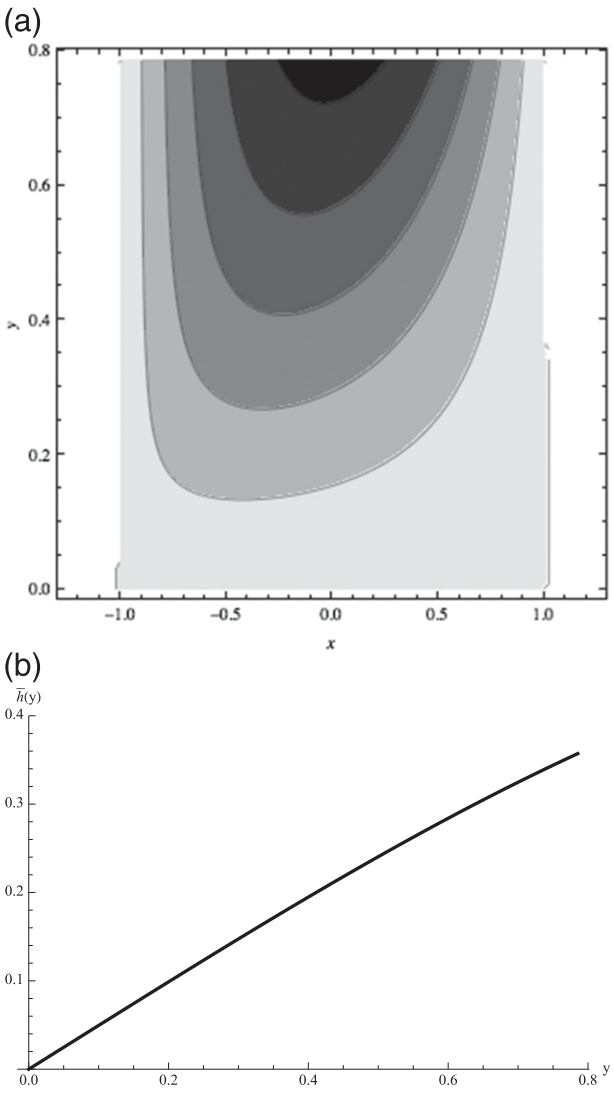


FIG. 4. (a) Contour plot of $h(x, y)$. The contour interval is about 0.1. (b) Graph of the zonally averaged abyssal layer height $\bar{h}(y)$ for $0 \le y \le y_0$.

behavior of the midlatitude zonal and meridional volume fluxes are finite as the equatorial region is approached, that is,

$$u(x,y)h(x,y) \approx -\frac{h_0^2[\tilde{\tau}(x)]}{\sin^2 y_0} \quad \text{and}$$

$$v(x,y)h(x,y) \approx \frac{h_B'(x) h_0[\tilde{\tau}(x)]}{\sin y_0}, \tag{57}$$

as $y \to 0$.

In addition, we note that the Coriolis terms in (8) and (9) will remain $O(1)$ for the midlatitude solution as the equatorial region is entered since

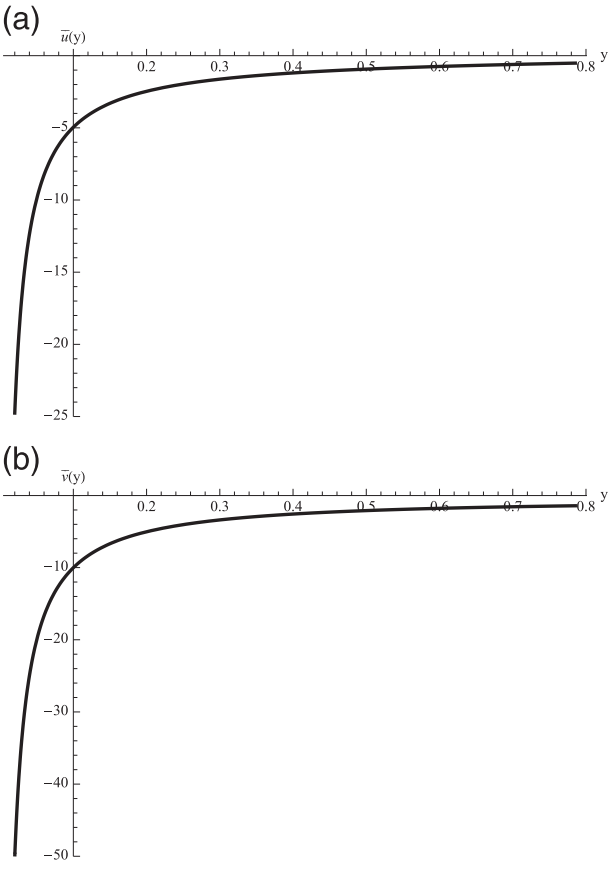


FIG. 5. For $0.02 \le y \le y_0$, zonally averaged (a) zonal velocity $\bar{u}(y)$ and (b) meridional velocity $\bar{v}(y)$.

$$\sin(y)u(x,y) \approx -\frac{h_0[\tilde{\tau}(x)]}{\sin y_0} \quad \text{and} \quad \sin(y)v(x,y) \approx h_B'(x), \tag{58}$$

as $y \to 0$.

Appreciating that $h(x, y) \simeq O(y)$ in the equatorial region, examining (8) and (9) suggests that the *first* distinguished limit of interest as $y \to 0$ will occur when there is a balance between the $\varepsilon v v_y$ term and the Coriolis term $\sin(y)u$ in (9) and this occurs for $y \simeq O(\varepsilon^{1/3}) \simeq O(0.14)$ or, dimensionally, in a zonal band with meridional width on the order of $\varepsilon^{1/3}R \simeq 885$ km centered along the equator.

To this end we introduce the "intermediate" (tilde) equatorial variables given by

$$u = \varepsilon^{-1/3}\tilde{u}(x,\xi), \quad v = \varepsilon^{-1/3}\tilde{v}(x,\xi),$$
$$h = \varepsilon^{1/3}\tilde{h}(x,\xi) \quad \text{and} \quad y = \varepsilon^{1/3}\xi, \tag{59}$$

into (8)–(10), yielding

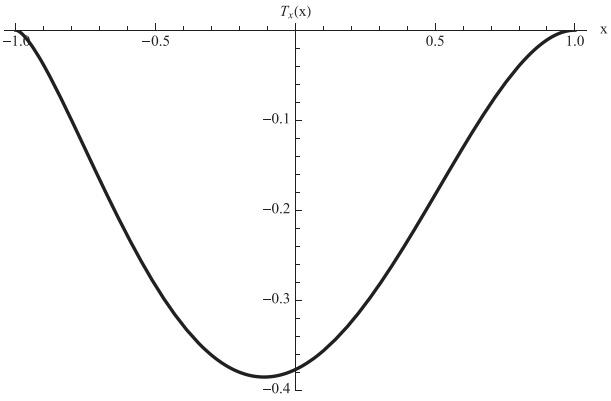


FIG. 6. Zonal transport $T_x(x)$ for $-1 \le x \le 1$.

$$\kappa^2(\varepsilon^{1/3}\tilde{u}\partial_x + \tilde{v}\partial_\xi)\tilde{u} - \frac{\sin(\varepsilon^{1/3}\xi)}{\varepsilon^{1/3}}\tilde{v}$$
$$= -(h_B + \varepsilon^{1/3}\tilde{h})_x + \frac{1}{\mathrm{Re}}(\varepsilon^{2/3}\partial_{xx} + \kappa^2\partial_{\xi\xi})\tilde{u}, \tag{60}$$
$$\varepsilon^{1/3}\tilde{u}\tilde{v}_x + \tilde{v}\tilde{v}_\xi + \frac{\sin(\varepsilon^{1/3}\xi)}{\varepsilon^{1/3}}\tilde{u}$$
$$= -\tilde{h}_\xi + \frac{1}{\kappa^2\mathrm{Re}}(\varepsilon^{2/3}\partial_{xx} + \kappa^2\partial_{\xi\xi})\tilde{v}, \quad \text{and} \tag{61}$$
$$\varepsilon^{1/3}(\tilde{u}\tilde{h})_x + (\tilde{v}\tilde{h})_\xi = 0. \tag{62}$$

Within the context $\kappa^2 \simeq \mathrm{Re}^{-1} \lesssim O(\varepsilon)$, it follows that the leading-order problem (as $\varepsilon \to 0$) associated with (60)–(62) will be the equatorial $\beta$-plane balance, given by

$$\xi\tilde{v} = h_B'(x), \tag{63}$$
$$\tilde{v}\tilde{v}_\xi + \xi\tilde{u} = -\tilde{h}_\xi, \quad \text{and} \tag{64}$$
$$(\tilde{v}\tilde{h})_\xi = 0, \tag{65}$$

which must be solved subject to the asymptotic matching conditions

$$\tilde{h} \to \frac{\xi h_0[\tilde{\tau}(x)]}{\sin y_0}, \tag{66}$$
$$\tilde{u} \to -\frac{h_0[\tilde{\tau}(x)]}{\xi \sin y_0}, \quad \text{and} \tag{67}$$
$$\tilde{v} \to \frac{h_B'(x)}{\xi}, \tag{68}$$

as $\xi \to \infty$ (in the case of the Southern Hemisphere where $y_0 < 0$, this would be replaced with $\xi \to -\infty$), where (66)–(68) are (54)–(56) written in terms of the "intermediate" equatorial variables in (59). Note that (63) and (68) are identical so that the solution for $\tilde{v}$ is given by (63).

The PV equation associated with the leading-order [(63)–(65)] is simply given by

$$\tilde{v}(\xi/\tilde{h})_{\xi} = 0,$$

which can be derived from first principles from the PV equation associated with (60)–(62) and letting $\varepsilon \to 0$, or directly by computing $\partial_{\xi}$ [(63)] and eliminating $\tilde{v}_{\xi}$ using (65).

Equations (63)–(65) imply that in the intermediate equatorial region the meridional velocity is geostrophically balanced solely against the topographic gradient [i.e., the DWBC height makes no contribution to the leading-order reduced pressure in (63)], the meridional volume flux is constant with respect to $\xi$, and the zonal velocity is determined by the Coriolis effect and the pressure gradient due to the DWBC height *and* the nonlinear correction associated with the northward advection of meridional momentum.

It follows from (65) and the matching conditions [(65) and (68)] that

$$\tilde{v}\tilde{h} = \tilde{v}\tilde{h}|_{\xi\to\infty} = \frac{h_B'(x)h_0[\tilde{\tau}(x)]}{\sin y_0}, \tag{69}$$

which, together with (63), implies that

$$\tilde{h}(x,\xi) = \frac{\xi h_0[\tilde{\tau}(x)]}{\sin y_0}, \tag{70}$$

which is, of course, identical to (66). Consequently, from (64), the zonal velocity will be determined by

$$\tilde{u}(x,\xi) = -\frac{1}{\xi}(\tilde{v}\tilde{v}_{\xi} + \tilde{h}_{\xi}) = \frac{1}{\xi}\left\{\frac{[h_B'(x)]^2}{\xi^3} - \frac{h_0[\tilde{\tau}(x)]}{\sin y_0}\right\}, \tag{71}$$

which will satisfy the leading-order matching condition [(67)].

The solution for $\tilde{u}$ has the property that the DWBC turns eastward (i.e., $\tilde{u} > 0$) for

$$0 < \xi < \xi_{\text{cross}}(x) \equiv \left\{\frac{[h_B'(x)]^2 \sin y_0}{h_0[\tilde{\tau}(x)]}\right\}^{1/3}, \tag{72}$$

assuming $y_0 > 0$ [and $0 > \xi > \xi_{\text{cross}}(x)$ for southern hemispheric flow where $y_0 < 0$]. Observe that $\xi_{\text{cross}}(x)$ depends inversely on the DWBC height $h_0[\tilde{\tau}(x)]$, meaning that the streamlines start to turn "eastward" farther away from the equator for smaller values of the height. This may be interpreted as a consequence of the fact that where the current has more momentum {i.e., for larger values of $h_0[\tilde{\tau}(x)]$} there is increased inertial penetration into the intermediate region before the flow turns eastward.

Written in terms of the outer or midlatitude variables [see (59)], the intermediate solutions of (63), (60), and (61) are given by

$$h_i(x,y) \equiv \varepsilon^{1/3}\tilde{h}(x, y/\varepsilon^{1/3}) = \frac{y h_0[\tilde{\tau}(x)]}{\sin y_0}, \tag{73}$$

$$u_i(x,y) \equiv \varepsilon^{-1/3}\tilde{u}(x, y/\varepsilon^{1/3}) = \frac{1}{y}\left\{\frac{\varepsilon[h_B'(x)]^2}{y^3} - \frac{h_0[\tilde{\tau}(x)]}{\sin y_0}\right\}, \tag{74}$$

and

$$v_i(x,y) \equiv \varepsilon^{-1/3}\tilde{v}(x, y/\varepsilon^{1/3}) = \frac{h_B'(x)}{y}, \tag{75}$$

with

$$y_{\text{cross}}(x) \equiv \varepsilon^{1/3}\xi_{\text{cross}}(x) = \left\{\frac{\varepsilon[h_B'(x)]^2 \sin y_0}{h_0[\tilde{\tau}(x)]}\right\}^{1/3}, \tag{76}$$

where the subscript "$i$" denotes "intermediate."

Figure 7a is a graph of $y_{\text{cross}}(x)$ versus $x$ for $-1 < x < 1$ assuming the parameter values in section 3b. Formally, $y_{\text{cross}}(x) \to \infty$ as $x \to \pm 1^{\mp}$ since $h_0[\tilde{\tau}(\pm 1^{\mp})] = h_0(\pm 1^{\mp}) = 0^{+}$ in (76). The minimum value of $y_{\text{cross}}(x)$ is about 0.16, which occurs at $x \simeq -0.42$ and is within $O(\delta)$ of the value of $x$ for which $\tilde{\tau}(x) = 0$ {i.e., the value that maximizes $h_0[\tilde{\tau}(x)]$}, which is given by $x = (1 - \sqrt{1 + 2\delta H})/\delta \simeq -0.52$.

To give an "average" representation of $u_i(x, y)$ over the interval $-1 < x < 1$, in Fig. 7b we show a graph of $\overline{u}_i(y)$ versus $y$ for $0.15 \le y \le 0.3$, where

$$\overline{u}_i(y) \equiv \frac{1}{2}\int_{-1}^{1} u_i(x,y)\,dx. \tag{77}$$

On average, in the intermediate region, the DWBC flows westward until about $y \simeq 0.17$, after which it starts to flow eastward in the equatorial region.

In Fig. 7c we show a plot of a selection of pathlines the flows takes as it enters the intermediate region. The pathlines, denoted as $y = y_{\text{path}}(x)$, were computed by numerically solving the equation

$$\frac{dy}{dx} = \frac{v_i(x,y)}{u_i(x,y)} = \frac{h_B'(x)}{\varepsilon[h_B'(x)]^2/y^3 - h_0[\tilde{\tau}(x)]/\sin y_0}, \tag{78}$$

subject to the "initial" condition

$$y(x_0) = y_0 \equiv 0.25, \tag{79}$$

where $-1 \le x_0 \le 1$ (all parameter values are those in section 3b). The initial value $y_0 \equiv 0.25$ is chosen to be

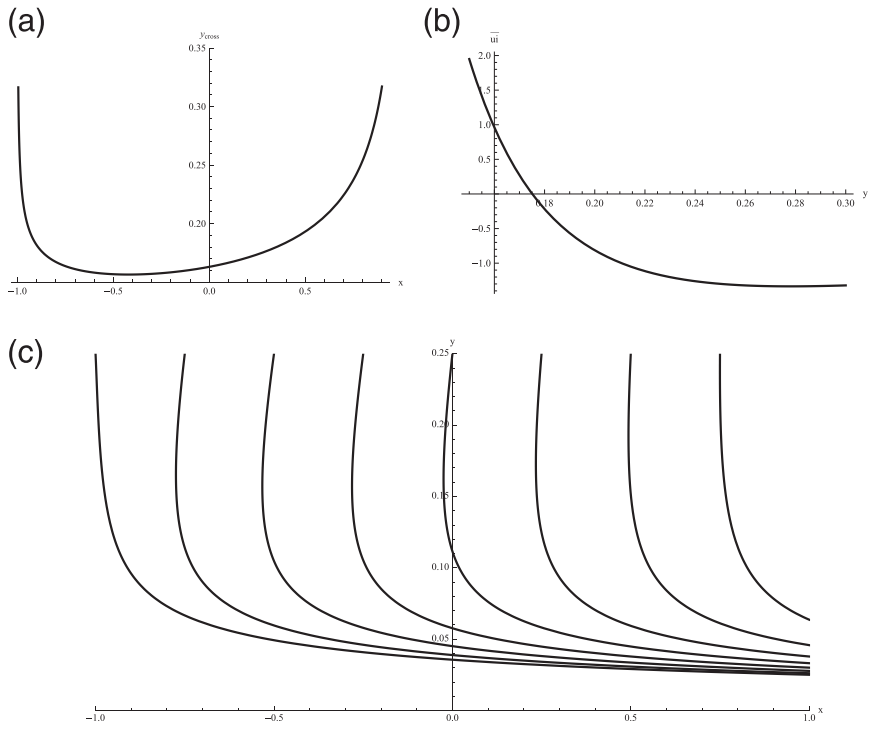


FIG. 7. (a) Graph of $y_{\text{cross}}(x)$ vs $x$ for $-1 \le x \le 1$. (b) Graph of $\overline{u}_{\text{i}}(y)$ vs $y$ for $0.15 \le y \le 0.3$. (c) Graph of the pathlines $y = y_{\text{path}}(x)$ as the flow enters the intermediate region.

"outside" the intermediate layer and $-1 \le x_0 \le 1$ is chosen to restrict attention to the region where $h_0[\tilde{\tau}(x)] > 0$. Figure 7c shows the pathlines associated with $x_0 = -1 + 0.25n$ for $n = 0, 1, \ldots, 7$.

As seen in Fig. 7c, the current enters the intermediate region flowing in the southwestward direction (consistent with the streamlines/characteristics shown in Fig. 3). In the region $0 < y < 0.15$, the flow has turned and is flowing eastward. Since the turn toward the east is a consequence of the term $[h_B'(x)]^2/\xi^4$ in (71) and this term is positive irrespective of the sign of $\xi$, the DWBC would turn eastward whether it was initially situated in the northern or the Southern Hemisphere. Figure 7c shows the flow narrowing as it turns eastward and developing into an equatorial jet, again, qualitatively consistent with the observations.

The intermediate region cannot describe cross-equatorial flow since the velocities $u_i(x, y)$ and $v_i(x, y)$ are unbounded as $y \to 0$ [see (74) and (75)]. Note that it follows from (78) that $dy/dx \to 0$ as $y \to 0$ along the pathlines so that the flow actually becomes parallel to the equator as the equator is approached. This behavior is clearly seen in Fig. 7c. The solutions for $h_i(x, y)$, $u_i(x, y)$ and $v_i(x, y)$ imply that any inertial equatorial and in particular any cross-equatorial flow with bounded velocities and nonzero thickness must be further resolved through an "inner" inertial equatorial boundary layer, which presumably exhibits a higher degree of nonlinearity. The intermediate layer examined here has, however, accomplished the important physics of turning the flow eastward into a zonally aligned equatorial jet. The dynamics in this "inner" inertial equatorial boundary layer is described in Part II.

## 5. Conclusions

A theoretical study of the nonlinear hemispheric-scale midlatitude and cross-equatorial steady-state dynamics of a grounded DWBC has been given. The spatial domain considered was a differentially rotating meridionally aligned basin with zonally varying parabolic bottom topography so that the model ocean shallows on both the western and eastern sides of the basin.

Away from the equator the flow was shown to be governed by a nonlinear planetary geostrophic balance in which the potential vorticity equation reduces to a quasi-linear hyperbolic equation that can be explicitly solved. The flow in midlatitudes exhibits increasing speed as the flow approaches the equator, consistent with the observations, and the DWBC height decreases (as a consequence of PV conservation). The flow in midlatitudes maintains a constant meridional volume transport with respect to latitude. In addition, there is a slight westward or upslope

transport induced in midlatitudes as the flow moves equatorward, which arises because of the planetary vorticity gradient.

As the flow enters the equatorial region, it becomes increasingly nonlinear and passes through two inertial boundary layers, which are referred to as the ''intermediate'' and ''inner'' inertial equatorial regions, respectively. The flow within the intermediate inertial equatorial boundary layer is resolved in this paper (Part I). For typical parameter values, the outer boundary of the intermediate region corresponds to a distance of about 885 km from the equator. Within the so-called intermediate region, the flow accelerates eastward as it flows equatorward, eventually becoming a predominately zonal jet. The qualitative properties of the midlatitude solution and the solution in the intermediate inertial boundary layer are consistent with the known behavior of the DWBC as it approaches the equator. However, within the intermediate inertial boundary layer, the current speeds within the DWBC continue to increase and the DWBC height continues to decrease as the intermediate region is traversed as the equator is further approached. This unphysical behavior is finally resolved in the inner equatorial region, which is described in Part II of this study.

*Acknowledgments.* Preparation of this manuscript was supported in part by Discovery Grants awarded by the Natural Sciences and Engineering Research Council (NSERC) of Canada.

## REFERENCES

Baehr, J., S. Cunningham, H. Haak, P. Heimbach, T. Kanzow, and J. Marotzke, 2009: Observed and simulated estimates of the meridional overturning circulation at 26.5°N in the Atlantic. *Ocean Sci.*, **5**, 575–589, doi:10.5194/os-5-575-2009.

Choboter, P. G., and G. E. Swaters, 2004: Shallow water modeling of Antarctic Bottom Water crossing the equator. *J. Geophys. Res.*, **109**, C03038, doi:10.1029/2003JC002048.

Cunningham, S. A., and Coauthors, 2007: Temporal variability of the Atlantic meridional overturning circulation at 26.5°N. *Science*, **317**, 935–938, doi:10.1126/science.1141304.

Dengler, M., F. A. Schott, C. Eden, P. Brandt, J. Fischer, and R. J. Zantopp, 2004: Break-up of the Atlantic deep western boundary current into eddies at 8°S. *Nature*, **432**, 1018–1020, doi:10.1038/nature03134.

Edwards, C. A., and J. Pedlosky, 1998a: Dynamics of nonlinear cross-equatorial flow. Part I: Potential vorticity transformation. *J. Phys. Oceanogr.*, **28**, 2382–2406, doi:10.1175/1520-0485(1998)028<2382:DONCEF>2.0.CO;2.

——, and ——, 1998b: Dynamics of nonlinear cross-equatorial flow. Part II: The tropically enhanced instability of the western boundary current. *J. Phys. Oceanogr.*, **28**, 2407–2417, doi:10.1175/1520-0485(1998)028<2407:DONCEF>2.0.CO;2.

Fischer, J., and F. A. Schott, 1997: Seasonal transport variability of the deep western boundary current in the equatorial Atlantic. *J. Geophys. Res.*, **102**, 27 751–27 769, doi:10.1029/97JC02327.

Gouriou, Y., and Coauthors, 2001: Deep circulation in the equatorial Atlantic ocean. *Geophys. Res. Lett.*, **28**, 819–822, doi:10.1029/2000GL012326.

Joyce, T. M., J. Dunworth-Baker, R. S. Pickart, and S. Waterman, 2005: On the deep western boundary current south of Cape Cod. *Deep-Sea Res. II*, **52**, 615–625, doi:10.1016/j.dsr2.2004.12.013.

Kim, A., G. E. Swaters, and B. R. Sutherland, 2014: Cross-equatorial flow of grounded abyssal ocean currents. *Geophys. Astrophys. Fluid Dyn.*, **108**, 363–386, doi:10.1080/03091929.2014.891023.

McCartney, M. S., 1993: Crossing of the equator by the deep western boundary current in the western Atlantic Ocean. *J. Phys. Oceanogr.*, **23**, 1953–1974, doi:10.1175/1520-0485(1993)023<1953:COTEBT>2.0.CO;2.

——, and R. A. Curry, 1993: Transequatorial flow of Antarctic Bottom Water in the western Atlantic Ocean: Abyssal geostrophy at the equator. *J. Phys. Oceanogr.*, **23**, 1264–1276, doi:10.1175/1520-0485(1993)023<1264:TFOABW>2.0.CO;2.

Nof, D., 1983: The translation of isolated cold eddies on a sloping bottom. *Deep-Sea Res.*, **30A**, 171–182, doi:10.1016/0198-0149(83)90067-5.

——, and S. Borisov, 1998: Inter-hemispheric oceanic exchange. *Quart. J. Roy. Meteor. Soc.*, **124**, 2829–2866, doi:10.1002/qj.49712455215.

Pedlosky, J., 1987: *Geophysical Fluid Dynamics*. 2nd ed. Springer, 710 pp.

Richardson, P. L., and D. M. Fratantoni, 1999: Float trajectories in the deep western boundary current and deep equatorial jets of the tropical Atlantic. *Deep-Sea Res. II*, **46**, 305–333, doi:10.1016/S0967-0645(98)00100-3.

Spall, M. A., 1994: Wave-induced abyssal recirculations. *J. Mar. Res.*, **52**, 1051–1080, doi:10.1357/0022240943076830.

Swaters, G. E., 2006a: The meridional flow of source-driven abyssal currents in a stratified basin with topography. Part I. Model development and dynamical characteristics. *J. Phys. Oceanogr.*, **36**, 335–355, doi:10.1175/JPO2855.1.

——, 2006b: The meridional flow of source-driven abyssal currents in a stratified basin with topography. Part II. Numerical simulation. *J. Phys. Oceanogr.*, **36**, 356–375, doi:10.1175/JPO2868.1.

——, 2013: Flow of grounded abyssal ocean currents along zonally-varying topography on a rotating sphere. *Geophys. Astrophys. Fluid Dyn.*, **107**, 564–586, doi:10.1080/03091929.2012.751381.

——, 2015: Midlatitude-equatorial dynamics of a grounded deep western boundary current in a meridional basin with parabolic bottom topography. Part II: Cross-equatorial dynamics. *J. Phys. Oceanogr.*, **45**, 2470–2483, doi:10.1175/JPO-D-14-0208.1.

Thierry, V., H. Mercier, and A. M. Treguier, 1998: Direct observations of low frequency fluctuations in the deep equatorial Atlantic. *Ann. Geophys.*, **16** (Suppl. 11), C568.

Toole, J. M., R. G. Curry, T. M. Joyce, M. McCartney, and B. Pena-Molino, 2011: Transport of the North Atlantic deep western boundary current about 39°N, 70°W: 2004–2008. *Deep-Sea Res. II*, **58**, 1768–1780, doi:10.1016/j.dsr2.2010.10.058.